Initial type and abundance of cyanobacteria determine morphotype development of phototrophic ecosystems

Esmee Joosten, Jérôme Hamelin, Kim Milferstedt

Accepted as Research Article in FEMS Microbiology Ecology, 2023, 97, 1–13, DOI: 10.1093/femsec/fiad099

Initial type and abundance of cyanobacteria determine morphotype development of phototrophic ecosystems

Esmee Desirée Joosten, Jérôme Hamelin*, Kim Milferstedt*

INRAE, Univ Montpellier, LBE, 102 Avenue des Etangs, 11100, Narbonne, France

*These authors contributed equally to this work

Corresponding author

Email: kim.milferstedt@inrae.fr

Phone: 0033 4 68 42 51 55

Abstract

Phototrophic aggregates containing filamentous cyanobacteria occur naturally, e.g. as cryoconite on glaciers and microbialites in fresh or marine waters, but their formation is not fully understood. Laboratory models are now available to reproduce aggregation, i.e. the formation of different morphotypes like hemispheroids, microbial mats, or sphere-like aggregates we call photogranules. In the model, activated sludge as starting matrix is transformed into aggregates enclosed by a phototrophic layer of growing cyanobacteria. These cyanobacteria were either enriched from the matrix or we added them intentionally. We hypothesize that the resulting morphotype depends on the type and concentration of the added cyanobacteria. When cyanobacteria from mature photogranules were added to activated sludge, photogranulation was not observed but microbial mats formed. Photogranulation of sludge could be promoted when adding sufficient quantities of cyanobacterial strains that form clumps when grown as isolates. The cyanobacteria putatively responsible for photogranulation were undetectable or only present in low abundance in the final communities of photogranules, that was always dominated by mat-forming cyanobacteria. We suggest that in a temporal succession, the ecosystem engineer initiating photogranulation eventually disappears, leaving behind its structural legacy. We conclude that understanding phototrophic aggregate formation requires considering the initial succession stages of the ecosystem development.

Keywords

cyanobacteria, bioaugmentation, phototrophic aggregate, photogranule, succession, ecosystem engineer

Introduction

Spherical, phototrophic aggregates are found in widely different habitats, ranging, among others, from cryoconite granules on glacier surfaces (Takeuchi, Nishiyama and Li 2010) to modern microbialites in tropical lagoons (Abed *et al.* 2003) or marine waters (Brehm, Krumbein and Palinska 2003). We are interested in this type of aggregates, as they may find use in biotechnological applications where organic compounds are oxidized, e.g. in wastewater treatment or resource recovery (Milferstedt *et al.* 2017). It is generally assumed that filamentous cyanobacteria play a major role in the spatial development of these aggregates, for example in cryoconites (Edwards *et al.* 2014; Anesio *et al.* 2017) and modern stromatolites (Reid *et al.* 2000; Foster *et al.* 2009). The most abundant cyanobacteria in mature cryoconite have been considered the ecosystem engineer for initiating cryoconite formation (Edwards *et al.* 2014; Anesio *et al.* 2017), but there is uncertainty about whether a specific genus or family is responsible for cryoconite formation (Gokul *et al.* 2016; Segawa *et al.* 2017; Uetake *et al.* 2019). This is in part due to the fact that it is intrinsically difficult to follow the spatial development of individual aggregates over time in natural environments. Additionally, unsuccessful aggregations will not develop a cryoconite granule and thus remain undetected. These limitations bias aggregation studies towards the successfully spatialized end products, disregarding the initial conditions of spatial developmental and aggregation failure.

Spatial organization is an often neglected topic in microbial ecology despite being an important property of many ecosystems (Widder *et al.* 2016). Spatial organization links microbial community structure to ecosystem function by favoring the development of substrate and metabolite gradients in the ecosystem (Momeni, Waite and Shou 2013). Investigating the relationship between spatial organization, microbial community assembly and ecosystem function contributes to the understanding of natural and engineered spatially explicit ecosystems.

It is possible to follow the formation of phototrophic aggregates in real-time in a lab-scale model system (Park, C. & Dolan 2019). Using this system, an organic matrix, typically fresh, untreated activated sludge, is exposed to light in a closed, hydrostatically incubated vial, i.e. the sludge bed was not agitated in any way. Over the course of several weeks, a spherical aggregate of several millimeters in diameter may form. In these aggregates, a growing, dense layer of mostly cyanobacteria confines the still unconsolidated organic matrix to the center of the aggregates (Milferstedt *et al.* 2017). We call these aggregates "oxygenic photogranules" to differentiate them from other naturally occurring phototrophic aggregates. The outer layer of photogranules resembles the layer surrounding stromatolites and cryoconites, also consisting of a cloth-like mat of filamentous cyanobacteria and extracellular polymeric substances. This layer holds together sediment and organic particles in a dense sphere (Reid *et al.* 2000; Andres and Reid 2006; Langford *et al.* 2010). As in natural system, also in photogranules this outer layer provides structural integrity to the aggregates (Golubic, Seong-Joo and Browne 2000; Kuo-Dahab *et al.* 2018). The microbial communities in photogranules harbor in high abundance at least one but often several types of cyanobacteria of Subsection III (Milferstedt *et al.* 2017) according to Bergey's Manual of Systematics of Archaea and Bacteria (Castenholz *et al.* 2015). Cyanobacteria found in cryoconite and microbialite outer layers also often belong to Subsection III (Christner, Kvitko and Reeve 2003; Foster *et al.* 2009; Segawa and Takeuchi 2010). These cyanobacteria are characterized by a filamentous morphology and often gliding motility. The strong similarity between photogranules and cryoconite was recently documented (Park and Takeuchi 2021). The ability of the lab-scale model system to reproduce similar spatial and community structures as in nature suggests its use as model system to study aggregation.

Our aim is to understand the initial role of cyanobacteria in the development of spatially organized ecosystems, notably in photogranules. In a controlled laboratory environment, it is possible to manipulate environmental conditions in individual incubations, e.g. the type and volume of the organic matrix, intensity

and spectrum of light, surface to volume ratios in the vials. However, consistent formation of spherical aggregates is not always observed, even in biological replicates (Joosten, Hamelin and Milferstedt 2020; Park and Takeuchi 2021). Instead, in addition to the photogranule structure, a wide range of spatial structures can be produced, including microbial mats and hemispheroids. We refer to these structures as morphotypes and to the diversity of structures within replicates in one experiment as morphotype distribution. External drivers like the induced defense of cyanobacteria against protozoan grazing may lead to spatialization by inducing clumping of the cyanobacteria (Fiałkowska and Pajdak–Stós 2002). Depending on the grazer concentration, cyanobacteria may form different morphotypes (Fyda, Fiałkowska and Pajdak-Stós 2010). This type of interaction is not the main focus of our experiments. However, it needs to be considered when interpreting observations from environments where protozoa may be present. Also in nature, a diversity of morphotypes formed by gliding filamentous cyanobacteria is documented, including flat mats (Stal 1995), rafts (Paerl, Bebout and Prufert 1989), tufts (Walter, Bauld and Brock 1976), clumps (Richardson and Castenholz 1989; Sim *et al.* 2012), and biological soil crust (Mazor *et al.* 1996; Garcia-Pichel *et al.* 2013).

For oxygenic photogranules, we postulate that the development of a spatial structure depends on the type and initial abundance of gliding filamentous cyanobacteria in the activated sludge. Filamentous cyanobacteria are typically rare in activated sludge, but account for large numbers of bacteria in final communities of all observed morphotypes (Milferstedt *et al.* 2017). Random differences in the initially low abundance and type of cyanobacteria in activated sludge may explain the unreproducible outcome between replicates. We hypothesized that we can redirect the outcome of the morphotype distribution towards any of the morphotypes by adding the appropriate gliding filamentous cyanobacteria to the inoculum.

We investigated how the modification of the type and initial abundance of cyanobacteria that is added to an organic matrix, i.e. here activated sludge, influenced the final spatial and community structure of the developing phototrophic ecosystem. We studied the initial and end point in the temporal succession, i.e. the replacement of the added cyanobacteria by other cyanobacteria, using partial 16S and 23S rRNA gene sequences in the final communities.

Materials and Methods

Hydrostatic production of morphotypes from augmented activated sludge

In five independent series of experiments, we transformed fresh, naturally non-phototropic, activated sludge into a phototrophic ecosystem (Figure 1). We used activated sludge as organic matrix because we know that this matrix can lead to the development of different morphotypes in hydrostatic batch cultivations. The origin of the activated sludge was in all three experiments the same aeration basin of the domestic wastewater treatment plant of Narbonne, France. Fresh activated sludge was sampled from the treatment plant at the start of each experiment. Experiments were conducted at three different times of the year over a period of three years (Table 1). Activated sludge was not treated to suppress protozoa and metazoan activity. An aliquot of the activated sludge samples was stored at -20°C until DNA extraction. No activated sludge samples are available for the first two experiments for technical reasons. The absolute abundance of phototrophs in activated sludge is typically low compared to the overall number of non-phototrophic bacteria (phototroph to non-phototroph ratio is 0.2 in sludges 3 and 4, and $4 \cdot 10^{-3}$ in sludge 5. We verified the low cyanobacterial abundance in samples taken two to three weeks later and took the results as a proxy for our samples. This is not ideal but acceptable in this specific situation considering the consistently low abundances close to the detection limit. We used different types of vessels for the transformation and inoculated different volumes of well-mixed activated sludge as a function of vessel volume (Table 1). Additions consisted either of serially diluted stock solutions prepared from (1) complex phototrophic communities (Figure 1: i – iii, ix), or (2) xenic cyanobacterial strains (Figure 1: iv – viii). Activated sludge

Table 1. Summary of experimental set-ups. *23S rRNA gene copies·ml^{-1} of most abundant cyanobacterial sequence types per addition.

Sludge Sampling date	**Type of vessel**	**Sludge volume (ml)**	**Sludge concentration (g·L^{-1})**	**Augmentation**	**Dilution**	**Cyanobacterial addition** (23S rRNA gene copies·ml^{-1})*	**Number of replicates**	**PAR (µmol·m^2·s^{-1})**
1 23 May 2016	24-well plates	2	3.5	-) control i) outer layers of OPGs	-) NA i) 10^6, 10^4, 10^2, 1	-) NA i) $1.2{\cdot}10^2$, $1.2{\cdot}10^4$, $1.2{\cdot}10^6$, $1.2{\cdot}10^8$	20 19	104
2 9 June 2016	24-well plates	2.4	3.5	-) control ii) outer layers of OPGs	-) NA ii) 10^6, 10^5, 10^4, $5{\cdot}10^3$, 10^3, 10^2, 10	-) NA ii) $6{\cdot}10^1$, $6{\cdot}10^2$, $6{\cdot}10^3$, $1.2{\cdot}10^4$, $6{\cdot}10^4$, $6{\cdot}10^5$, $6{\cdot}10^6$	12	104
3 19 Dec. 2017	4 ml vial	1.5	4.9 ± 0.1 (n=3)	-) control iii) entire OPGs	-) NA iii) 10^6, 10^4, 10^2	-) NA iii) $1.3{\cdot}10^4$, $1.3{\cdot}10^6$, $1.3{\cdot}10^8$	18	78
4 3 July 2019	10 ml vial	7	4.3 ± 0.1 (n=3)	-) control iv) *O. lutea* SAG 1459-3	-) NA iv) 10^2, 50, 10	-) NA iv) $2.7{\cdot}10^6$, $5.4{\cdot}10^6$, $2.5{\cdot}10^7$	9	78
5 4 Sept. 2019	10 ml vial	7	4.9 ± 0.1 (n=3)	-) control iv) *O. lutea* SAG 1459-3 v) *Kamptonema*- vi) *Planktothrix*- vii) *Nodosilinea*-like strain viii) unclassified cyanobacterial strain ix) outer layer of OPG	-) NA iv) $5{\cdot}10^5$, 10 v) 10^4, 10 vi) $1.6{\cdot}10^3$, 10 vii) $2.3{\cdot}10^5$, 10 viii) $0.7{\cdot}10^3$, 10 ix) 1	-) NA iv) $1.3{\cdot}10^3$, $6.5{\cdot}10^7$ v) $1.3{\cdot}10^5$, $1.2{\cdot}10^8$ vi) $1.5{\cdot}10^5$, $2.4{\cdot}10^7$ vii) $1.1{\cdot}10^4$, $2.5{\cdot}10^8$ viii) $4.2{\cdot}10^5$, $3.1{\cdot}10^7$ ix) $4.7{\cdot}10^7$	32 16	78

was well-mixed on a magnetic stirrer. The additions were homogenized using a micropestle for Eppendorf tubes (i-iii, ix) or disperser (T-25 Ultra-Turrax, IKA-Werke GmbH & Co. KG, Staufen, Germany) (iv-viii). Sludges 1-5 were incubated as controls, i.e., without addition, or with added cyanobacteria at different concentrations. See Table 1 for a detailed summary. Microplates and vials were subsequently closed to prevent evaporation. The vessels were hydrostatically incubated at room temperature under constant warm white LED illumination at 78 $\mu mol \cdot m^{-2} \cdot s^{-1}$ photosynthetically active radiation (PAR) for vials (i.e. sludge 3-5) and a PAR of 104 $\mu mol \cdot m^{-2} \cdot s^{-1}$ for microplates (i.e. sludge 1, 2). Vials and microplates were not touched or moved during the experiment, and the sludge was not agitated in any way. Each series of vials was incubated until compact phototrophic morphotypes developed that remained intact when vigorously shaken. This was typically the case after two to eight weeks. We quantified morphotype formation by automatically capturing biomass diameter as a measure for contraction using time-lapse imaging (Joosten, Hamelin and Milferstedt 2020), based on a method used for cryoconite quantification (Irvine-Fynn, Bridge and Hodson 2010). Cyanobacterial addition did not change the speed of contraction of a sludge (t-test; Figure S1). We supplemented the time-lapse imaging data with pictures and descriptions of the final morphotype that formed in each vessel, i.e. a microbial mat, hemispheroid or spherical photogranule (Figure 1). We consider a microbial mat a flat and compacted structure that covers the entire bottom of the vessel. A hemispheroid is contracted, i.e. it covers a smaller area than the vessel bottom and has a curved surface. A photogranule has a smaller contact area with the vessel bottom than the apparent diameter of the biomass aggregate. Its self-supporting morphology resembles a spheroid (Milferstedt *et al.* 2017). We verified the presence of filamentous cyanobacteria using stereomicroscopy (M205FA, Leica Microsystems SAS, Nanterre, France) with white light as well by phycocyanin autofluorescence using an ET535/50x and ET590 LP filter set. Samples were stored at -20°C until DNA extraction.

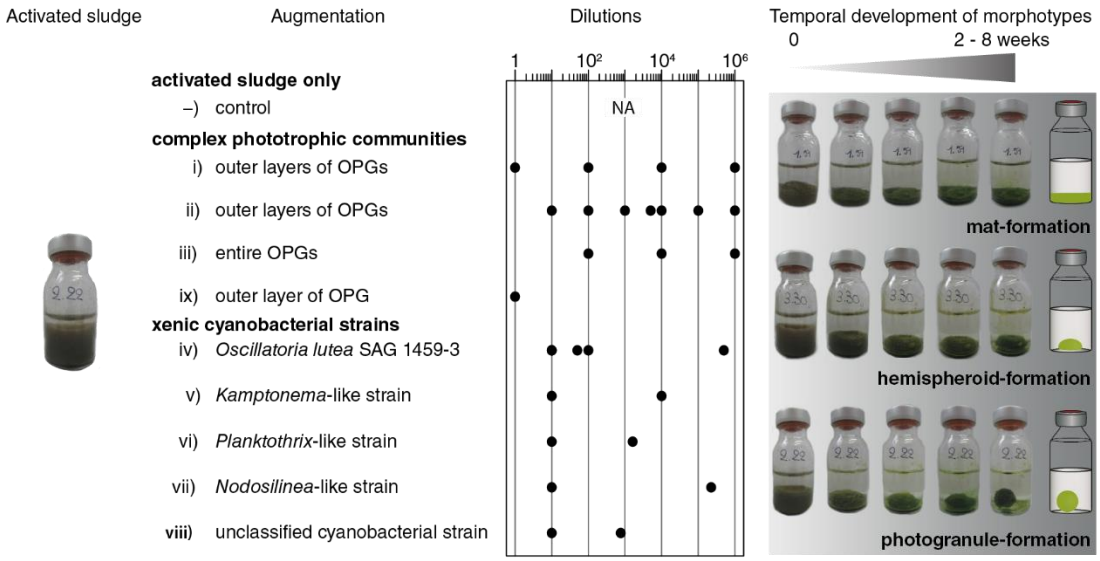

Figure 1. Schematic representation of the experiments in which activated sludge was augmented with cyanobacteria to influence morphotype development. The description of the biomass used for the additions is given, as well as the dilutions that we used. The type of addition is listed by decreasing complexity. The photo shows exemplary temporal developments of the mat-forming, hemispheroid-forming and photogranule-forming morphotypes in 10 ml vials, together with a schematic representation of the final morphotype. The transformation of the untreated or augmented activated sludge could result in a single morphotype, or in a range of morphotypes.

Production of biomass for addition to activated sludge

Complex phototrophic communities

Phototrophic communities to be added to activated sludge were produced using published procedures (Milferstedt *et al.* 2017; Joosten, Hamelin and Milferstedt 2020). From the photogranules, the outer layers were peeled off (Figure 1: i, ii, ix) (Supplementary Information) or used entirely (Figure 1: iii) and manually homogenized with a micropestle. The homogenized solutions were the starting point for serial dilutions that were used straightaway to be added to the sludge (Table 1). Cyanobacterial stock solutions and dilutions were stored at -20°C until DNA extraction. Dominant cyanobacteria in the phototrophic communities were a *Tychonema* sequence type (additions i, ii, ix), or a *Pantanalinema* sequence type (addition iii).

Xenic cyanobacterial strains

The strain *Oscillatoria lutea* SAG 1459-3 (addition iv) was ordered from the Culture Collection of Algae at the University of Göttingen, Germany (http://sagdb.uni-goettingen.de/). Other xenic cyanobacterial strains used to add to activated sludge (Figure 1: v – iii) were isolated from mature photogranules at the Muséum National d'Histoire Naturelle (MNHN), Paris, France. Single cyanobacterial filaments were separated from different photogranules and transferred to fresh Z8 medium (Kotai 1972). Cyanobacterial strains in the additions were identified by sequencing as a *Kamptonema*-like (v), *Planktothrix*-like (vi), *Nodosilinea*-like strain (vii) and an unclassified cyanobacterium (viii) (Table S1). All the strains belong to Subsection III: non-heterocystous, unbranched filamentous cyanobacteria of which most exhibit gliding motility (Castenholz *et al.* 2015). Gliding motility of the strains was confirmed by plating and microscopic observations. Cyanobacterial strains were grown in BG-11 medium (Rippka, Deruelles and Waterbury 1979) at 12/12-hour light/dark cycles at 30 $\mu mol \cdot m^{-2} \cdot s^{-1}$ PAR. Cyanobacterial biomass was homogenized with a disperser one day before being added to the activated sludge. These stock solutions were kept in suspension using magnetic stirring. Two to three dilutions were prepared and added to the sludge (Table 1). The dilution steps were adjusted to the estimated concentrations of the stock solutions to obtain similar cell numbers (Table 1) and later quantified using qPCR. Cyanobacterial dilutions were stored at -20°C until DNA extraction.

Determination of microbial community structure

DNA was extracted from all samples using DNeasy PowerWater Kit (Qiagen GmbH, Hilden, Germany) following the manufacturer's instructions. DNA concentration and purity were determined by spectrophotometry (Spark NanoQuant M10, Tecan, Männedorf, Switzerland). Extracted DNA was stored at -20°C.

Microbial quantification by qPCR

Concentrations of bacteria and cyanobacteria in all samples were determined by qPCR with universal bacterial primers and primers specific for cyanobacteria (including chloroplasts). DNA extracts were diluted to a concentration of 10 $ng \cdot \mu l^{-1}$. Universal bacterial primers targeting the V3-V4 regions of the 16S rRNA gene were used. Reaction mixtures contained 2.5 µl of SsoAdvanced™ Universal Probes Supermix (Bio-rad Laboratories, Hercules, CA, USA), 100 nM of forward primer BAC338F (5'-ACTCCTACGGGA-GGCAG-3'), 250 nM of reverse primer BAC805R (5'-GACTACAGGGTATCTAAT CC-3'), 50 nM of probe BAC516F (5'-Yakima Yellow-TGCCAGCAGCCGCGGTAATAC–TAMRA-3') (Yu *et al.* 2005) and 1 µl of DNA for a final volume of 5 µl. The qPCR program consisted of 2 min at 95°C for pre-incubation of the DNA template, followed by 40 cycles of 7 s at 95°C for denaturation and 25 s at 60°C for annealing and amplification. Cyanobacterial primers targeted the V2-V3 regions of the 16S rRNA gene of

cyanobacteria and chloroplasts. Reaction mixtures contained 12.5 µl of SsoAdvanced™ Universal Probes Supermix, 200 nM of forward primer CYAN 108F (5'- ACGGGTGAGTAACRCGTRA-3'), 200 nM of reverse primer CYAN 377R (5'- CCATGGCGGAAAATTCCC-3') (Urbach, Robertson and Chrisholm 1992; Nübel, Garcia-Pichel and Muyzer 1997) and 2 µl of DNA for a final volume of 12.5 µl. The qPCR program consisted of 2 min at 95°C for pre-incubation of the DNA template, followed by 40 cycles of 15 s at 95°C for denaturation and 60 s at 52°C for annealing and amplification, followed by melting curve analysis. Samples were treated using a Bravo automated liquid handling platform (Agilent, Santa Clara, CA, USA) and a ViiA 7 384-wells real-time PCR system (Applied Biosystems, Waltham, MA, USA) at the GeT-Trix platform of GenoToul Genopole Toulouse, France.

Microbial community sequencing

Amplicons of 16S (bacteria and archaea) and 23S (cyanobacteria and chloroplasts) rRNA gene fragments were sequenced to determine the microbial community composition. The V4-V5 regions of the 16S rRNA gene was PCR amplified using the primer pair U515-532F 5′-GTGYCAGCMGCCGCGGTA-3′ and U909-928R 5′-CCCCGYCAATTCMTTTRAGT-3′ (Wang and Qian 2009) with their respective linkers over 30 cycles (annealing temperature 65°C). These primers target both bacterial (including cyanobacteria and chloroplasts) and archaeal 16S rRNA genes. The same DNA was amplified with the primer pair p23SrV_f1 5′-GGACAGAAAGACCCTATGAA-3′ and p23SrV_r1 5′-CAGCCTGTTATCCCTAGAG-3′ (Sherwood and Presting 2007) with their respective linkers over 30 cycles (annealing temperature 59°C). These primers target a 23S rDNA plastid marker in cyanobacteria and eukaryotic algae.

DNA amplicons were submitted for sequencing of paired 300 bp reads according to the manufacturer's instructions (Illumina MiSeq v3 chemistry, San Diego, CA, USA) to the GeT-PlaGe sequencing platform of GenoToul Genopole Toulouse, France. The amplicon sequences of 3 out of 5 activated sludge sources (not available for sludge 1 and 2), 12 cyanobacterial additions and 68 final morphotypes are available in the NCBI Sequence Read Archive under BioProject number PRJNA849163.

Forward and reverse reads were assembled using a modified version of the MiSeq Standard Operating Procedure (Kozich *et al.* 2013) in Mothur version 1.42.3 (Schloss *et al.* 2009). This included pre-clustering at four differences in nucleotides over the length of the amplicon and chimera checking using UCHIME (Edgar *et al.* 2011). Rare unique sequences that appeared less than three times in the entire data set were removed. Taxonomic alignment of 16S and 23S sequences was done to the respective SILVA databases SSURef and LSURef, release 132 (Quast *et al.* 2013), as provided by Mothur. Based on their taxonomy, 16S sequences were separated into bacterial and archaeal sequences, and 23S into cyanobacterial and chloroplast sequences.

Operational taxonomic units (OTUs) represented unique sequences after cleaning. Relative sequence counts were transformed to absolute counts using qPCR results by combining copy numbers of bacteria and cyanobacteria for 16S sequence counts and using cyanobacterial copy numbers alone for 23S sequence counts.

Sequence data were analyzed in R 4.0.3 (R Core Team 2020) using *phyloseq* 1.27.6 (McMurdie and Holmes 2013). We analyzed the change in microbial community structure from untreated or augmented activated sludge to final morphotypes. We tested whether morphotypes had different community structures using *adonis* (pairwise permutational multivariate analysis of variance) from *vegan* 2.5-6 (Oksanen *et al.* 2019) on the Bray-Curtis distance matrix. Homogeneity of dispersion between groups of samples needs to be assured as it is a prerequisite for a valid comparison of morphotypes using *adonis*. For this, we performed *betadisper* from vegan on the Bray-Curtis distance matrix to test if groups of samples (i.e. morphotypes) were homogenously dispersed in relation to their OTUs in the samples (Anderson 2006).

Ternary plots

From the 23S sequence data, we selected the sequences identified as cyanobacteria and grouped them by the respective affiliation to Subsection according to Bergey's Manual of Systematics of Archaea and Bacteria (Castenholz *et al.* 2015). We divided cyanobacterial sequences from Subsection III into four categories based on taxonomy: (1) photogranule-formers (*Oscillatoria* and *Kamptonema* sequences), (2) hemispheroid-formers (*Planktothrix* sequences), (3) mat-formers (*Tychonema*, *Nodosilinea*, and sequences identical to that of the isolated, unclassified cyanobacterium strain), (4) sequence types that did not fit into the previous three categories. We plotted in an equilateral triangle, i.e. a ternary plot, the relative abundances of the first three groups, i.e. photogranule-formers, hemispheroid-formers and mat-formers at two time points: (1) at the beginning of the experiment (activated sludge without or with cyanobacterial addition) and (2) in the final communities of the mature morphotypes. The sum of these three groups equals one in the plots. The successional development of the cyanobacteria is indicated as the trajectories between initial and final communities.

Results and Discussion

Morphotype development in untreated activated sludge

We use for all of our experiments activated sludge as starting matrix to be enclosed by growing cyanobacteria. Activated sludge has been shown in to promote photogranulation, but also the formation of other morphotypes. Activated sludge is therefore a pragmatic choice for our experiments. It is likely possible to find a matrix that more closely resembles that of for example cryoconite or microbialites, or other ecosystems of interest.

We introduce in the following the aggregation behavior of activated sludge without any addition of cyanobacteria. The initial activated sludge we used consisted of small flocs below 100 µm in size. It was unconsolidated, i.e. entirely resuspendable after agitation. Over the course of several weeks, the sludge in each vial of an incubation set, i.e. all vials incubated with the same inoculum on the same day, transformed into a well-defined, macroscopic spatial structure. We classify the structures as either microbial mats, hemispheroids or photogranules (Figure 1). Each incubation set may lead to the development of one of these morphotypes, or a distribution of the morphotypes at varying abundances. With our five independent experiment we were able to cover a wide range of outputs. Three untreated sludge sources developed into a single morphotype, i.e. 100% photogranules (Figure 2: sludge 1, 2) or 100% mats (Figure 2: sludge 4). Two control sludge sources developed all three morphotypes, either being mat-dominated (Figure 2: sludge 3) or with approximately equal weights of the three morphotypes (Figure 3: sludge 5).

The development of photogranules over days and weeks must not be confused with aggregation behavior of cyanobacteria that is observed on time scales of minutes to hours in sufficiently dense cyanobacterial cultures (Castenholz 1967; Walsby 1968; Biddanda *et al.* 2015). In these situations, depending on initial trichome density, gliding cyanobacterial trichomes collide and get entangled in their matrix of EPS, leading to macroscopic structures (Castenholz 1967; Walsby 1968; Shepard and Sumner 2010; Tamulonis and Kaandorp 2014). Instead, during photogranulation, cyanobacterial growth is needed to build the phototrophic layer that eventually transforms a predominantly heterotrophic ecosystem into a spatially explicit syntrophic ecosystem.

To examine the effect of adding cyanobacteria to activated sludge, we first analyzed the occurrence of cyanobacteria in the initial organic matrix, i.e. activated sludge. The biological and chemical composition of the initial activated sludge differed per experiment due to natural variation. Based on qPCR results, the bacterial community of activated sludge in the five experiments was almost entirely composed of non-

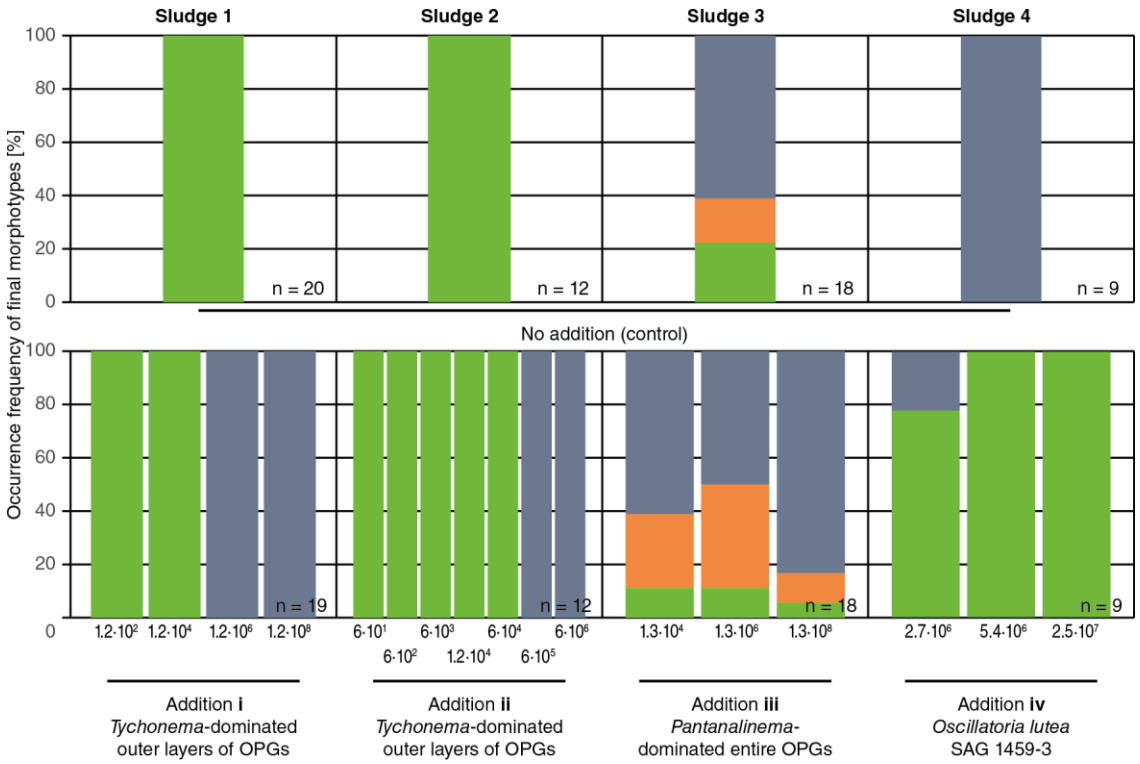

Figure 2. Modification of the morphotype-forming behavior of untreated activated sludge after cyanobacterial augmentation. Increasing cyanobacterial additions are expressed in 23S rRNA gene copies·ml^{-1} of the most dominant cyanobacterial sequence type per addition, *i.e.* (**i-ii**) *Tychonema*, (**iii**) *Pantanalinema* and (**iv**) *Oscillatoria lutea*. Resulting morphotypes are presented as percentage of the number of replicates in bar plots: spherical photogranules are shown in green, hemispheroids in orange and microbial mats in blue-gray.

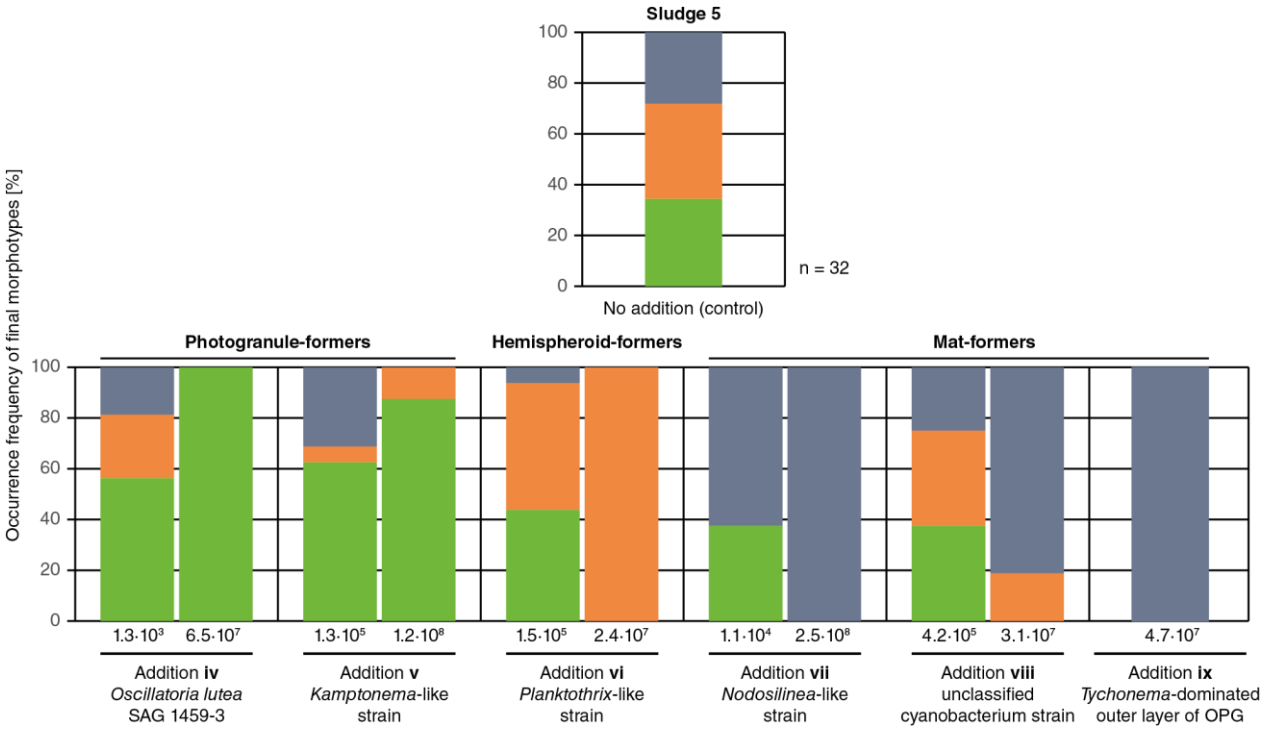

Figure 3. Directed modification of the morphotype-forming behavior of an untreated activated sludge after specific cyanobacterial augmentations. Note that addition **iv** contains the same strain as addition **iv** in **Figure 2**. Increasing cyanobacterial

additions are expressed in 23S rRNA gene copies·ml^{-1} of the (most dominant) cyanobacterial sequence type per addition, *i.e.* (**iv**) *Oscillatoria lutea*, (**v**) *Kamptonema*, (**vi**) *Planktothrix*, (**vii**) *Nodosilinea*, (**viii**) unclassified cyanobacterium and (**ix**) *Tychonema*. Resulting morphotypes are presented as percentage of the number of replicates in bar plots: spherical photogranules are shown in green, hemispheroids in orange and microbial mats in blue-gray. The number of replicates is 16 for all additions.

phototropic bacteria (98.6 ± 0.8%). Phototrophic microorganisms constituted a small part of the community (0.3 ± 0.4% cyanobacteria and 1.0 ± 0.5% eukaryotic algae (based on chloroplasts)). This is expected for activated sludge (Yang *et al.* 2011; Milferstedt *et al.* 2017). We did not study the eukaryotic community of activated sludge. The initial communities were analyzed at the beginning of three out of five experiments (not available for sludge 1 and 2). The phototrophic community in sludge 3 was dominated by an uncultured coccoidal *Chroococcidiopsis* (44% of cyanobacterial counts; representing only 0.1% of total bacterial counts), based on 23S rRNA gene amplicons. The filamentous cyanobacterium *Planktothricoides* dominated the phototrophic populations of sludge 4 and 5 (respectively, 49% and 79% of cyanobacterial counts; 0.4% and 0.002% of total bacterial counts). The cyanobacterial types detected in the inoculum remained rare after the transformation into phototrophic ecosystems. Cyanobacteria were enriched during morphotype development, making up on average 35 ± 15% of all bacteria and phototrophs in the final microbial communities. Eukaryotic algae constituted 4 ± 4% of the final communities and the remainder were non-phototrophic bacteria (61 ± 15%). No bacterial OTU was substantially selected during the experiments, with major bacterial OTUs representing less than 5.2 ± 6.4% of the total community (Supplementary Information). A single cyanobacterial OTU, however, could make up to 32 ± 19% of the total community. The substantial increase in cyanobacterial counts justifies our focus on cyanobacteria.

Morphotype development from activated sludge after cyanobacterial addition

We initially hypothesized that the ability to form a photogranule can be attributed to cyanobacteria in the photogranule outer layer. Following this, we should have been able to then propagate the ability to form photogranules from one generation of photogranules to the next. To test this, we added phototrophic communities coming from the outer layers peeled off from mature photogranules or entire mature photogranules to the initial activated sludge. Resulting from this addition, we were able to modify the spatial self-organization of the developing phototrophic ecosystems. However, unexpectedly large additions of outer layers of photogranules (Figure 1: addition i, ii) converted the naturally photogranule-forming sludge into a mat morphotype (Figure 2: sludge 1, 2; addition i, ii). Outer layers of photogranules were dominated by *Tychonema* sequence types at, respectively, 47% and 87% of cyanobacterial and 7% and 42% of total bacterial abundance. Adding entire photogranules (Figure 1: addition iii) to the dominantly mat-forming sludge likewise increased the proportion of mats in the resulting morphotypes compared to the control (Figure 2: sludge 3, addition iii). The additions with entire photogranules were dominated by a *Pantanalinema* sequence type at 100% of cyanobacterial and 48% of total bacterial abundance. In the initial sludge biomass, a *Pantanalinema*-like sequence type was already present at 0.03% of the initial activated sludge community, which corresponds to 12% of the initial cyanobacterial population. This is the only case in which the added sequence type was already present in the initial activated sludge. Contrary to our expectations, adding photogranule communities from (outer layers of) mature photogranules did not lead to the formation of photogranules.

One drawback of working with additions of cyanobacteria-dominated communities derived from the outer layers of photogranules is that these communities may already contain a variety of cyanobacterial strains, as well as other microorganisms, e.g. protozoa. In these more complex additions, potential antagonistic behavior between strains or other interactions, i.e. induced defense against ciliate grazing, makes the interpretation of these experiments more difficult. We therefore simplified the experiment by adding a xenic *Oscillatoria lutea* strain belonging to Subsection III from a culture collection. Adding the *Oscillatoria lutea*

(Figure 1: addition iv) to an initially mat-forming sludge directed morphotype development towards photogranules (Figure 2: sludge 4, addition iv). It is thus possible to shift morphotype development towards photogranulation.

To gain insight into which cyanobacteria in photogranules are responsible for spherical structure formation in the hydrostatic batch ecosystem, we isolated xenic cyanobacterial strains from the outer layers of mature photogranules. We were able to isolate a *Kamptonema*-like, *Planktothrix*-like, *Nodosilinea*-like and unclassified cyanobacterium strain. When adding cyanobacterial strains to an activated sludge that produced an approximately equal distribution of morphotypes (Figure 3: sludge 5), we were able to push the spatial development towards a single morphotype, depending on the type and abundance of the added strain. The addition of *Oscillatoria lutea* and *Kamptonema* directed morphotype development towards photogranules (Figure 3: addition iv, v). This corresponds to what we observed for *Oscillatoria lutea* when added to sludge 4 (Figure 2: addition iv). The addition of the *Planktothrix*-like strain resulted in the dominance of the hemispheroid morphotype (Figure 3: addition vi). This is the only strain we isolated that leads to the formation of hemispheroids. Adding *Nodosilinea* and the unclassified cyanobacterium to activated sludge 5 led to a mat-dominated distribution (Figure 3: addition vii, viii). The shift towards mat formation was equally observed for *Tychonema*-dominated additions (Figure 3: addition ix). This corresponds to what we observed for the *Tychonema*-dominated additions to sludge 1 and 2 (Figure 2: addition i, ii). We could thus redirect morphotype development as a function of the added cyanobacterial strain.

Morphotypes of cyanobacterial strains in culture medium

When growing the cyanobacterial isolates in Z8 or BG11 culture medium, i.e. without the addition of an external matrix (activated sludge), we observed that the xenic cyanobacterial strains grown as isolates develop a similar morphotype as their phototrophic aggregate after transformation of activated sludge (Figure 4). The *Kamptonema*-like strain 3 (Figure 4a), as do *Kamptonema animale* SAG 1459-6 and *Kamptonema formosum* PCC 6407 (Figure 4c, d, respectively), as well as the culture collection strain *Oscillatoria lutea* SAG 1459-3 (Figure 4b) formed aggregates resembling photogranules. Note that the latter two *Kamptonema* strains were not used for augmentation experiments in this manuscript. In addition to this phenotypic similarity, the *Kamptonema*-like isolate is also phylogenetically closely related to *O. lutea* SAG 1459-3 and *Kamptonema* sp. (data not shown). The 23S rRNA amplicon of the *Kamptonema*-like isolate shared 95.9% sequence identity with *O. lutea* SAG 1459-3 and 98.7% with the two *Kamptonema* culture collection strains.

The *Planktothrix*-like strain built elongated, free-floating aggregates (Figure 4e). Note that we called these structures “hemispheroid” in 10 ml vials of the batch cultivation system because in these vials the biomass was in contact with the bottom of the vial. When growing as isolates in Erlenmeyer flasks, the floating biomass is not limited by the glass bottom, and therefore is more “elongated”.

The *Nodosilinea*-like strain formed biofilms covering the water-glass interface with pillars extending from the biofilm into the bulk liquid (Figure 4f). The unclassified cyanobacterium strain built patchy biofilms (Figure 4g). A *Tychonema*-like strain formed a somewhat smooth biofilm covering the entire air-water interface (Figure 4h). Its 23S rRNA sequence was identical to the *Tychonema* sequence types found in additions i, ii and ix. The identified mat-forming strains were phylogenetically more distantly related to each other (between 84.1 and 87.5%) than the photogranule-forming strains of *Oscillatoria* and *Kamptonema*.

Cyanobacterial type and abundance determine morphotype development

We observed the reproducible formation of a specific morphotype after addition of a specific cyanobacterial strain and therefore hypothesize that morphotype formation is strain-dependent. Based on our experience,

we consider the *Tychonema, Pantanalinema, Nodosilinea* sequence types, as well as the unclassified cyanobacterium strain mat-formers. Our *Planktothrix* sequence types are hemispheroid-formers and *Kamptonema* and *Oscillatoria* sequence types are considered photogranule-formers.

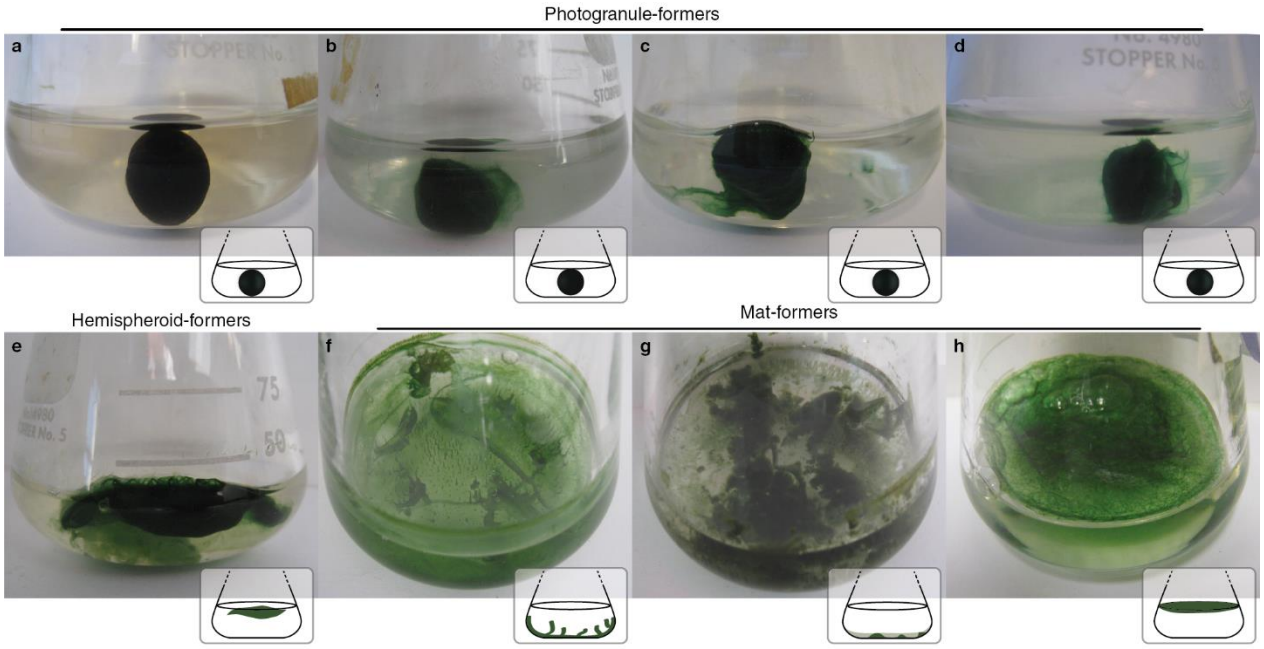

Figure 4. Macroscopic structures formed by xenic cyanobacterial cultures. Cyanobacterial cultures in Z8 or BG-11 culture medium in 125 ml Erlenmeyer flasks. Photogranule-formers: (a) *Kamptonema*-like strain, (b) *Oscillatoria lutea* SAG 1459-3, (c) *Kamptonema animale* SAG 1459-6, (d) *Kamptonema formosum* PCC 6407. (e) *Planktothrix*-like strain forming elongated structures or hemispheroids. Mat-formers: (f) *Nodosilinea*-like strain, (g) unclassified cyanobacterium strain, (h) *Tychonema*-like strain.

The ecosystem-wide impact of cyanobacterial additions depends on the initial cyanobacterial concentration added to the matrix. With increasing numbers of added cells (Figure 2, Figure 3), the distribution of morphotypes shifted towards the morphotype that was preferentially produced by the dominant cyanobacterium in the addition. The number of cells needed to induce a shift in morphotypes is not fixed, but may depend on the already present autochthonous cyanobacterial population of the activated sludge. The concentration-dependent shift in spatial structure formation was most clearly visible after the addition of outer layers dominated by the putative mat-former *Tychonema* to a naturally photogranule-forming sludge (Figure 2: addition i, ii; Figure S1). Photogranules were still produced after small additions of *Tychonema*-dominated outer layers, whereas greater additions led to the formation of microbial mats. The shift towards mat formation was also observed after we added *Tychonema*-dominated communities (Figure 3: addition ix) to an activated sludge that produced a wider range of morphotypes.

Increasing additions of the mat-former *Pantanalinema* to a mostly mat-producing sludge increased the proportion of mats among the morphotypes (Figure 2: addition iii). This was also true when other mat-forming cyanobacteria were added (Figure 3: addition vii, viii). The same concentration-dependency was observed for the hemispheroid-forming (Figure 3: addition vi) and photogranule-forming strains (Figure 2, Figure 3: addition iv, v). A minimum dose of cyanobacteria is thus needed to be able to colonize and grow in the new environment. A larger immigrating community has a higher chance of invading a new environment, because it is less likely to disappear due to stochastic events. Larger invading communities typically also contain more species diversity and can therefore adapt faster to their new environment (Lockwood, Cassey and Blackburn 2005; Sierocinski *et al.* 2021). Spatial structuring can additionally help to sustain the invaders by creating a separate niche that prevents interaction with the residents (Castledine

et al. 2020). The outcome of mixing communities, i.e. the resulting community, can differ for each mixing event. *Tychonema*-dominated outer layers of photogranules had a lasting effect on morphology after smaller additions compared to *Oscillatoria lutea* SAG 1459-3. This is possibly related to the greater species diversity and relatedness (Castledine *et al.* 2020) to the photogranule environment of the phototrophic community compared to the culture collection strain.

Photogranulation a result of induced defenses against grazing?

In the literature, spatial arrangement of filamentous cyanobacteria is reported to result from an induced defense against protozoan grazing (Fiałkowska and Pajdak–Stós 1997)(Fiałkowska and Pajdak–Stós 1997)(Fiałkowska and Pajdak–Stós 1997)(Fiałkowska and Pajdak–Stós 1997). On the order of minutes to hours, filamentous cyanobacteria of the genus *Phormidium* confronted with a high number of certain ciliates formed dense and stable clumps with spatial dimensions reaching several millimeters (Pajdak-Stós, Fiałkowska and Fyda 2001). Without strong grazing pressure, a mat like structure was formed (Pajdak-Stós, Fiałkowska and Fyda 2001). The resemblance of these structures with what we observed in our experiments is undeniable and provokes the question of how grazing may be involved in photogranulation. Our experiments were not designed to evaluate this hypothesis and we did not quantify protozoan abundance or activity in our incubations. Grazing protozoa were occasionally microscopically detected in our samples, but not in excessive numbers. Fiałkowska and Pajdak–Stós (2002) postulated a dynamic predator-prey relationship in which the abundance of the cyanobacteria and ciliates oscillates, followed by an equally dynamic morphology of the phototrophic aggregates between open and dense structures. This behavior has not yet been observed in photogranules. Instead, once formed, the spatial structures persisted over periods of several weeks, possibly pointing towards other, or additional drivers than grazing. All xenic cyanobacterial strains that were used in our experiments form a specific morphotype when grown as isolates in synthetic medium (Figure 4). Ciliates have not been observed in these cultures so that an influence of grazing on their morphotype development can be excluded. However, after mixing with activated sludge, the consequences of the exposure to a wide range of potential grazers on photogranulation need to be evaluated in a carefully designed experiment. Exposure to grazers is unavoidable in open reactors for biotechnological applications and therefore deserves our attention.

Added cyanobacteria act as ecosystem engineer

The morphotype developed by the isolated cyanobacterial strains is carried over to augmented sludge when the respective morphotype is added in sufficiently large quantities. From our observations, it follows that the properties of the added cyanobacterial strain determine the final spatial structure of the developing ecosystem. The cyanobacteria harbor a physiological trait, i.e. determining the morphotype, that is imprinted on the sludge. The added cyanobacteria provoke a change in the ecosystem behavior that exceeds what is expected based on their abundance. Even the largest cyanobacterial addition of $2.5 \cdot 10^8$ 23S rRNA gene copies$\cdot$ml^{-1} represented only 0.5% of the total number of cells. The added cyanobacteria can be considered as ecosystem engineer of the spatial assembly of these phototrophic ecosystems since its contribution to the final morphotype was notable even at low concentration (Power *et al.* 1996). Phylogenetically and morphologically similar gliding filamentous cyanobacteria also act as ecosystem engineer in nature, e.g. when forming biological soil crust in desert ecosystems (Mazor *et al.* 1996; Garcia-Pichel *et al.* 2013) or cryoconite on glacier surfaces (Edwards *et al.* 2014; Anesio *et al.* 2017).

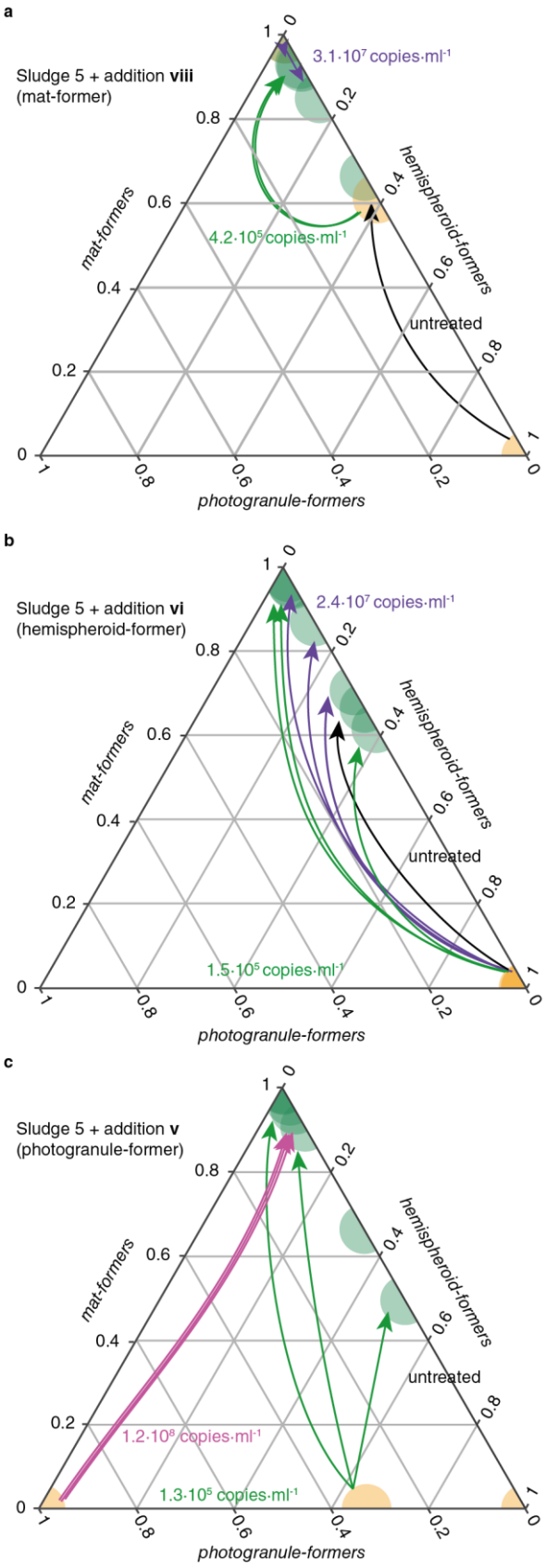

Figure 5. Representative changes in proportion of mat-, hemispheroid- and photogranule-formers from the inoculum to the final morphotype communities. Sludge 5 augmented with (a) addition **viii**, (b) addition **vi** and (c) addition **v**. Results are based on 23S rRNA gene amplicon sequencing and cyanobacterial qPCR. The sum of mat-, hemispheroid- and photogranule-formers equals 1. Initial activated sludge is shown in orange and final morphotypes in green. Arrows indicate the temporal transition from initial activated sludge, without (black arrow) or with cyanobacterial addition (colored arrows), to final morphotype community. Same colored arrows indicate replicates on a single image (n=2-3), and the same order of magnitude of the cyanobacterial addition between images (green: 10^5, purple: 10^7, pink: 10^8 23S rRNA gene copies·ml^{-1}).

Cyanobacterial succession during morphotype development

We initially assumed that the added strains would end up or even be enriched in the final communities. We therefore investigated how initial cyanobacterial additions modified the final microbial community structure. The arrows in the ternary plots visualize the shift in abundance of photogranule-, hemispheroid-, and mat-formers from the initial to the final communities for the untreated and augmented sludge (Figure 5, Figure S2). We observed that the morphotype-formers always had a higher abundance in the final communities than in the initial communities. We consistently observed that eventually, in the final spatial structures, mat-formers dominated the communities, independent of the added morphotype-former (Figure 5, Figure S2bce). This is visible by the arrows that point towards the top of the triangles in the ternary plots, indicating a high relative abundance of mat-formers in the final communities. Notable exceptions were the *Pantanalinema*-dominated addition of $1.3 \cdot 10^4$ copies$\cdot$ml^{-1} (addition iii) to sludge 3 for which each of the morphotype-formers dominated at least one of the replicates (Figure S2a: blue arrows), and the *Oscillatoria lutea* SAG 1459-3 addition (addition iv) to sludge 4 (Figure S2d), where sometimes also hemispheroid-formers became most abundant. Photogranule-formers were detected at most at low abundances or entirely undetectable in the final communities (Figure 5c, Figure S2de), despite having induced a morphological change. Final cyanobacterial communities of mats, hemispheroids and photogranules within an experiment were not significantly different from each other (*adonis* analysis). Microbial communities of mature aggregates thus do not allow us to trace back the cyanobacteria that were initially added to the activated sludge matrix.

Our results indicate that the final morphotype of an incubation results from the interaction between the added cyanobacteria and the cyanobacteria already present in the matrix. After small additions of cyanobacteria, whether they were mat-, hemispheroid-, or photogranule-formers, the autochthonous activated sludge community was not sufficiently affected and maintained the strongest impact on the final spatial structure. With an increasing number of added cells, the invader cyanobacteria could establish themselves in the ecosystem and override the otherwise naturally developing morphotype. We were unable to determine a generally valid number of added cells that induce a change in morphotype development. The number likely depends on the type and initial concentration of cyanobacteria present in the activated sludge matrix, as well as the type of the added cyanobacteria. However, independent of the number of added cells, it appears that during the development of the final morphotype, photogranule-formers eventually systematically disappeared, despite their marked effect in the earlier succession phase. Mat-formers were more competitive in the developing spatial structure, which may be related to the faster growth of *Tychonema*-like strains (in defined medium) compared to the *Kamptonema*-like strain (Table S2).

The ability of photogranule-formers to form photogranules may dependent on the expression of genes, e.g. those involved in gliding motility (Lamparter *et al.* 2022), filament flexibility-rigidity (Springstein *et al.* 2020) and binding ability (Pereira *et al.* 2015), that are not present or expressed in mat-formers. Solving this unknown is out of the scope of this study but whole-genome sequencing and transcriptomics during the spatialization may help identifying what factors drive the relationship between cyanobacterial types and spatialization. Alternatively, it may be possible that photogranule-formers induce a change in the activities of mat-formers that subsequently leads to photogranulation. If this was true, photogranule-formers may not necessarily play a direct role in structure building, but rather promote behavior in other community members (Mohlin *et al.* 2012) to form photogranules. This could have happened when photogranule-formers were still present (Chen *et al.* 2006) or after they had disappeared, i.e. by means of a microbial legacy effect (Leroy and De Vuyst 2004). In addition to a possibly modified behavior of mat-formers by substances secreted by photogranule-formers, photogranule-formers could leave behind a physical structure composed of empty sheaths. This structure may subsequently be inhabited by other microorganisms, e.g. mat-formers.

Validating these hypotheses, however, requires dedicated experiments. The fact that the putative ecosystem engineer must be initially present but may not dominate or even survive at the end of the process is also observed in other ecosystems, as for example in cheese production (Vass and Langenheder 2017). There, the ecosystem engineer is needed to ferment and acidify the milk to create a favorable habitat for the community involved in product maturation. Eventually, in the final product, starter microbes have a low abundance. As in cheese production, also in in the morphotype development of phototrophic ecosystems a succession of microbes, here cyanobacteria, can be observed.

We do not know at what point in photogranule development the added photogranule-formers like *Kamptonema* disappeared. It seems reasonable to assume that *Kamptonema* disappeared after the photogranule structure was built, i.e. after the photogranule morphotype was first observed. The stable structure of empty sheaths and exopolymers that was produced by *Kamptonema* could have been successively colonized by mat-forming cyanobacteria (Kühl, Fenchel and Kazmierczak 2003). We could have possibly detected *Kamptonema* in photogranules when sampling the photogranules when we first observe them, as opposed to our conservative sampling approach in which we waited for mature structures to be formed and stabilized in all vials before sampling. Alternatively, it may be that *Kamptonema* disappeared before we first observed the photogranule structure. This effect is similar to the impact of pioneering cyanobacteria that initiate the colonization and stabilization of natural ecosystems, including desert (Danin *et al.* 1998) and polar biological soil crusts (Pessi *et al.* 2019). These specialists are favored initially when cyanobacterial population density and competition are low. When environmental conditions change, specialists are outcompeted by generalists that are adapted to a wider range of environmental conditions (Sigler and Zeyer 2004). Cyanobacterial succession has been observed in eutrophic water bodies as a result of changing temperature (Chu *et al.* 2007), irradiance (Oberhaus *et al.* 2007), CO_2 (Van de Waal *et al.* 2011) or nutrient levels (Ammar *et al.* 2014).

It is desirable to monitor cyanobacterial succession during photogranulation. However, this is experimentally difficult as currently only destructive sampling allows microbial community analysis. Knowing that the development of a range of morphotypes is possible, it would thus be required to predict with certainty the final morphotype of the sacrificed incubation, which has so far not been possible. In our work, we demonstrated that we are able to control the morphological outcome by cyanobacterial augmentation with the appropriate strains. This allows us to design future experiments in which we can for example vary the number of added *Kamptonema* and *Tychonema* cells to investigate cyanobacterial competition at the tipping point between photogranule and mat formation. A detailed study of the physiology related to spatialization coupled to individual based modelling may help deciphering the different roles of these cyanobacteria in spatial structure formation (Kreft *et al.* 2007; Estrela and Brown 2013).

Photogranulation ability not shared between all Subsection III cyanobacteria

The identified photogranule-formers share high similarity between ribosomal gene sequences. They are phylogenetically close compared to the more diverse mat-formers. This may be the result of a sampling bias, because we isolated cyanobacteria from mature photogranules that typically contained a low number of photogranule-formers (Figure 5). Future isolation attempts should therefore consider the putative succession of cyanobacteria in photogranulating samples and include sampling at earlier stages, as the final community may only contain in low numbers the organisms responsible for structure development. A phylogenetically more diverse range of photogranule-formers could possibly be isolated at a time point better suited for photogranule-formers. If not, phylogenetically closely related photogranule-formers may imply that there is a narrow group of cyanobacteria that can form photogranules. Being able to produce photogranules may not be as common among Subsection III cyanobacteria as initially suggested (Milferstedt *et al.* 2017). There might also be a narrower group of Subsection III cyanobacteria responsible for the initiation of cryoconite

formation, which share similarities with photogranules (Park and Takeuchi 2021) and in which Subsection III members are typically believed to be ecosystem engineers (Gokul *et al.* 2016).

Our initial hypothesis that all cyanobacteria present in the outer layer of mature photogranules form this particular spherical structure oversimplified the process of photogranulation of biological material when it contains a diverse cyanobacterial community. Sufficiently large additions of phototrophic communities or xenic cyanobacterial strains to activated sludge led to a change in the distribution of morphotypes towards dominance of the morphotype typically formed by the added strain. Additions of lower numbers of the same organisms did not shift the distribution towards the expected morphotype (Figure 2 and 3). It seems that independent of the initial community structure and additions, including situations where photogranule-formers were added, mat-forming cyanobacteria eventually overrule other morphotype-formers. However, despite their eventual displacement from the phototrophic population, photogranule-formers like *Kamptonema* were the ecosystem engineers and shaped the final ecosystem structure as their relatively small addition led to a change in the distribution of morphotypes towards photogranules. If the disappearance of photogranule-formers from the final communities also applies to naturally occurring photogranules, studies of the final microbial communities, e.g. of already formed cryoconite, do not give insight into the ecosystem engineers responsible for their structure development. Laboratory studies, considering succession and multiple genome analyses of photogranule- and mat-formers, may advance our understanding of photogranulation and more generally the formation of phototrophic aggregates.

Acknowledgements

We thank Cécile Bernard, Charlotte Duval and Sahima Hamlaoui from Muséum National d'Histoire Naturelle (MNHN) of Paris for hosting and training E.D.J. on isolation of the xenic cyanobacterial strains. Without their expertise and help, we would not have been able to make the trait-based classification of the xenic strains. We thank Claire Naylies and Gaëlle Santa-Catalina for qPCR. This work benefited from the Environmental Biotechnology and Biorefinery Facility (Bio2E) of INRAE-LBE (doi.org/10.15454/1.557234103446854E12) and the Genome and Transcriptome facility (GeT) of Toulouse.

Funding

This work was funded through the Graduate School GAIA of Montpellier University of Excellence (PhD fellowship E.D.J.) and the National French Funding Agency ANR project PSST ANR-16-CE04-0001.

Contributions

All authors conceived the study, conducted the experiments and analyzed the data. E.D.J. wrote the manuscript. All authors contributed to revisions and approved the final version.

Competing Interests

The authors declare no conflict of interest.

Data Availability Statement

All data generated and analyzed during this study are included in this published article and its Supplementary Information files. The amplicon sequences are available in the NCBI Sequence Read Archive BioProject PRJNA849163 at https://www.ncbi.nlm.nih.gov/bioproject/PRJNA849163.

References

Abed RMM, Golubic S, Garcia-Pichel F *et al.* Characterization of microbialite-forming cyanobacteria in a tropical lagoon: Tikehau Atoll, Tuamotu, French Polynesia. *J Phycol* 2003;**39**:862–73.

Ammar M, Comte K, Tran TDC *et al.* Initial growth phases of two bloom-forming cyanobacteria (*Cylindrospermopsis raciborskii* and *Planktothrix agardhii*) in monocultures and mixed cultures depending on light and nutrient conditions. *Int J Limnol* 2014;**50**:231–40.

Anderson MJ. Distance-based tests for homogeneity of multivariate dispersions. *Biometrics* 2006;**62**:245–53.

Andres MS, Reid RP. Growth morphologies of modern marine stromatolites: a case study from Highborne Cay, Bahamas. *Sediment Geol* 2006;**185**:319–28.

Anesio AM, Lutz S, Chrismas NAM *et al.* The microbiome of glaciers and ice sheets. *npj Biofilms Microbiomes* 2017;**3**:1–11.

Biddanda BA, McMillan AC, Long SA *et al.* Seeking sunlight: rapid phototactic motility of filamentous mat-forming cyanobacteria optimize photosynthesis and enhance carbon burial in Lake Huron's submerged sinkholes. *Front Microbiol* 2015;**6**:1–13.

Brehm U, Krumbein WE, Palinska KA. Microbial spheres: a novel cyanobacterial-diatom symbiosis. *Naturwissenschaften* 2003;**90**:136–40.

Castenholz RW. Aggregation in a thermophilic *Oscillatoria*. *Nature* 1967;**215**:1285–6.

Castenholz RW, Rippka R, Herdman M *et al.* Subsection III. *Bergey's Man Syst Archaea Bact* 2015:1–4.

Castledine M, Sierocinski P, Padfield D *et al.* Community coalescence: an eco-evolutionary perspective. *Philos Trans R Soc B* 2020;**375**:20190252.

Chen B-Y, Chen S-Y, Lin M-Y *et al.* Exploring bioaugmentation strategies for azo-dye decolorization using a mixed consortium of *Pseudomonas luteola* and *Escherichia coli*. *Process Biochem* 2006;**41**:1574–81.

Christner BC, Kvitko BH, Reeve JN. Molecular identification of Bacteria and Eukarya inhabiting an Antarctic cryoconite hole. *Extremophiles* 2003;**7**:177–83.

Chu Z, Jin X, Iwami N *et al.* The effect of temperature on growth characteristics and competitions of *Microcystis aeruginosa* and *Oscillatoria mougeotii* in a shallow, eutrophic lake simulator system. *Eutrophication of Shallow Lakes with Special Reference to Lake Taihu, China*. Springer Dordrecht, 2007, 217–23.

Danin A, Dor I, Sandler A *et al.* Desert crust morphology and its relations to microbiotic succession at Mt. Sedom, Israel. *J Arid Environ* 1998;**38**:161–74.

Edgar RC, Haas BJ, Clemente JC *et al.* UCHIME improves sensitivity and speed of chimera detection. *Bioinformatics* 2011;**27**:2194–200.

Edwards A, Mur LAJ, Girdwood SE *et al.* Coupled cryoconite ecosystem structure-function relationships are revealed by comparing bacterial communities in alpine and Arctic glaciers. *FEMS Microbiol Ecol* 2014;**89**:222–37.

Estrela S, Brown SP. Metabolic and demographic feedbacks shape the emergent spatial structure and function of microbial communities. *PLoS Comput Biol* 2013;**9**:e1003398.

Fiałkowska E, Pajdak–Stós A. Inducible defence against a ciliate grazer *Pseudomicrothorax dubius*, in two strains of *Phormidium* (cyanobacteria). *Proc R Soc London Ser B Biol Sci* 1997;**264**:937–41.

Fiałkowska E, Pajdak–Stós A. Dependence of cyanobacteria defense mode on grazer pressure. *Aquat*

Microb Ecol 2002;**27**:149–57.

Foster JS, Green SJ, Ahrendt SR *et al.* Molecular and morphological characterization of cyanobacterial diversity in the stromatolites of Highborne Cay, Bahamas. *ISME J* 2009;**3**:573–87.

Fyda J, Fiałkowska E, Pajdak-Stós A. Dynamics of cyanobacteria–ciliate grazer activity in bitrophic and tritrophic microcosms. *Aquat Microb Ecol* 2010;**59**:45–53.

Garcia-Pichel F, Loza V, Marusenko Y *et al.* Temperature drives the continental-scale distribution of key microbes in topsoil communities. *Science (80-)* 2013;**340**:1574–7.

Gokul JK, Hodson AJ, Saetnan ER *et al.* Taxon interactions control the distributions of cryoconite bacteria colonizing a High Arctic ice cap. *Mol Ecol* 2016;**25**:3752–67.

Golubic S, Seong-Joo L, Browne KM. Cyanobacteria: architects of sedimentary structures. In: Riding RE, Awramik SM (eds.). *Microbial Sediments*. Berlin, Heidelberg: Springer, 2000, 57–67.

Irvine-Fynn TDL, Bridge JW, Hodson AJ. Rapid quantification of cryoconite: granule geometry and in situ supraglacial extents, using examples from Svalbard and Greenland. *J Glaciol* 2010;**56**:297–308.

Joosten ED, Hamelin J, Milferstedt K. Simple time-lapse imaging for quantifying the hydrostatic production of oxygenic photogranules. *Bio-Protocol* 2020;**10**:e3784.

Kotai J. Instructions for preparation of modified nutrient solution Z8 for algae. *Nor Inst Water Res Oslo* 1972;**11**:5.

Kozich JJ, Westcott SL, Baxter NT *et al.* Development of a dual-index sequencing strategy and curation pipeline for analyzing amplicon sequence data on the MiSeq Illumina sequencing platform. *Appl Environ Microbiol* 2013;**79**:5112–20.

Kreft J-U, Picioreanu C, Wimpenny JWT *et al.* Individual-based modelling of biofilms. *Microbiology* 2007;**147**:2897–912.

Kühl M, Fenchel T, Kazmierczak J. Growth, structure and calcification potential of an artificial cyanobacterial mat. *Fossil and Recent Biofilms, a Natural History of Life on Planet Earth*. Springer Dordrecht, 2003, 77–102.

Kuo-Dahab WC, Stauch-White K, Butler CS *et al.* Investigation of the fate and dynamics of extracellular polymeric substances (EPS) during sludge-based photogranulation under hydrostatic conditions. *Environ Sci Technol* 2018;**52**:10462–71.

Lamparter T, Babian J, Fröhlich K *et al.* The involvement of type IV pili and phytochrome in gliding motility, lateral motility and phototaxis of the cyanobacterium *Phormidium lacuna*. *PLoS One* 2022;**17**:e0249509.

Langford H, Hodson A, Banwart S *et al.* The microstructure and biogeochemistry of Arctic cryoconite granules. *Ann Glaciol* 2010;**51**:87–94.

Leroy F, De Vuyst L. Lactic acid bacteria as functional starter cultures for the food fermentation industry. *Trends Food Sci Technol* 2004;**15**:67–78.

Lockwood JL, Cassey P, Blackburn T. The role of propagule pressure in explaining species invasions. *Trends Ecol Evol* 2005;**20**:223–8.

Mazor G, Kidron GJ, Vonshak A *et al.* The role of cyanobacterial exopolysaccharides in structuring desert microbial crusts. *FEMS Microbiol Ecol* 1996;**21**:121–30.

McMurdie PJ, Holmes S. Phyloseq: an R package for reproducible interactive analysis and graphics of microbiome census data. *PLoS One* 2013;**8**:e61217.

Milferstedt K, Kuo-Dahab WC, Butler CS *et al.* The importance of filamentous cyanobacteria in the

development of oxygenic photogranules. *Sci Rep* 2017;**7**:17944.

Mohlin M, Roleda MY, Pattanaik B *et al.* Interspecific resource competition-combined effects of radiation and nutrient limitation on two diazotrophic filamentous cyanobacteria. *Microb Ecol* 2012;**63**:736–50.

Momeni B, Waite AJ, Shou W. Spatial self-organization favors heterotypic cooperation over cheating. *Elife* 2013;**2**:e00960.

Nübel U, Garcia-Pichel F, Muyzer G. PCR primers to amplify 16S rRNA genes from cyanobacteria. *Appl Environ Microbiol* 1997;**63**:3327–32.

Oberhaus L, Briand JF, Leboulanger C *et al.* Comparative effects of the quality and quantity of light and temperature on the growth of *Planktothrix agardhii* and *P. rubescens*. *J P* 2007;**43**:1191–9.

Oksanen J, Blanchet F, Friendly M *et al.* vegan: community ecology package. *R Package* 2019.

Paerl HW, Bebout BM, Prufert LE. Bacterial associations with marine *Oscillatoria* sp. (*Trichodesmium* sp.) populations: ecophysiological implications. *J Phycol* 1989;**25**:773–84.

Pajdak-Stós A, Fiałkowska E, Fyda J. *Phormidium autumnale* (Cyanobacteria) defense against three ciliate grazer species. *Aquat Microb Ecol* 2001;**23**:237–44.

Park, C. & Dolan S. Algal-sludge granule for wastewater treatment and bioenergy feedstock generation. 2019.

Park C, Takeuchi N. Unmasking photogranulation in decreasing glacial albedo and net autotrophic wastewater treatment. *Environ Microbiol* 2021;**23**:6391–404.

Pereira SB, Mota R, Vieira CP *et al.* Phylum-wide analysis of genes/ proteins related to the last steps of assembly and export of extracellular polymeric substances (EPS) in cyanobacteria. *Sci Rep* 2015;**5**:1–16.

Pessi IS, Pushkareva E, Lara Y *et al.* Marked succession of cyanobacterial communities following glacier retreat in the High Arctic. *Microb Ecol* 2019;**77**:136–47.

Power ME, Tilman D, Estes JA *et al.* Challenges in the quest for keystones: identifying keystone species is difficult—but essential to understanding how loss of species will affect ecosystems. *Bioscience* 1996;**46**:609–20.

Quast C, Pruesse E, Yilmaz P *et al.* The SILVA ribosomal RNA gene database project: improved data processing and web-based tools. *Nucleic Acids Res* 2013;**41**:590–6.

R Core Team. R: A language and environment for statistical computing. *R Found Stat Comput Vienna, Austria* 2020:https://www.r-project.org/.

Reid RP, Visscher PT, Decho AW *et al.* The role of microbes in accretion, lamination and early lithification of modern marine stromatolites. *Nature* 2000;**406**:989–92.

Richardson LL, Castenholz RW. Chemokinetic motility responses of the cyanobacterium *Oscillatoria terebriformis*. *Appl Environ Microbiol* 1989;**55**:261–3.

Rippka R, Deruelles J, Waterbury JB. Generic assignments, strain histories and properties of pure cultures of cyanobacteria. *J Gen Microbiol* 1979;**111**:1–61.

Schloss PD, Westcott SL, Ryabin T *et al.* Introducing mothur: open-source, platform-independent, community-supported software for describing and comparing microbial communities. *Appl Environ Microbiol* 2009;**75**:7537–41.

Segawa T, Takeuchi N. Cyanobacterial communities on Qiyi glacier, Qilian Shan, China. *Ann Glaciol* 2010;**51**:135–44.

Segawa T, Yonezawa T, Edwards A *et al.* Biogeography of cryoconite forming cyanobacteria on polar and Asian glaciers. *J Biogeogr* 2017;**44**:2849–61.

Shepard RN, Sumner DY. Undirected motility of filamentous cyanobacteria produces reticulate mats. *Geobiology* 2010;**8**:179–90.

Sherwood AR, Presting GG. Universal primers amplify a 23S rDNA plastid marker in eukaryotic algae and cyanobacteria. *J Phycol* 2007;**43**:605–8.

Sierocinski P, Pascual JS, Padfield D *et al.* The impact of invader number on whole community invasions in biomethane-producing communities. *Iscience* 2021;**24**:102659.

Sigler W V, Zeyer J. Colony-forming analysis of bacterial community succession in deglaciated soils indicates pioneer stress-tolerant opportunists. *Microb Ecol* 2004;**48**:316–23.

Sim MS, Liang B, Petroff AP *et al.* Oxygen-dependent morphogenesis of modern clumped photosynthetic mats and implications for the archean stromatolite record. *Geosciences* 2012;**2**:235–59.

Springstein BL, Woehle C, Weissenbach J *et al.* Identification and characterization of novel filament-forming proteins in cyanobacteria. *Sci Rep* 2020;**10**:1–17.

Stal LJ. Physiological ecology of cyanobacteria in microbial mats and other communities. *New Phytol* 1995;**131**:1–32.

Takeuchi N, Nishiyama H, Li Z. Structure and formation process of cryoconite granules on Ürümqi glacier No. 1, Tien Shan, China. *Ann Glaciol* 2010;**51**:9–14.

Tamulonis C, Kaandorp J. A model of filamentous cyanobacteria leading to reticulate pattern formation. *Life* 2014;**4**:433–56.

Uetake J, Nagatsuka N, Onuma Y *et al.* Bacterial community changes with granule size in cryoconite and their susceptibility to exogenous nutrients on NW Greenland glaciers. *FEMS Microbiol Ecol* 2019;**95**:fiz075.

Urbach E, Robertson DL, Chrisholm SW. Multiple evolutionary origins of prochlorophytes, the chlorophyll b-containing prokaryotes. *Nature* 1992;**355**:265–7.

Vass M, Langenheder S. The legacy of the past: effects of historical processes on microbial metacommunities. *Aquat Microb Ecol* 2017;**79**:13–9.

Van de Waal DB, Verspagen JMH, Finke JF *et al.* Reversal in competitive dominance of a toxic versus non-toxic cyanobacterium in response to rising CO_2. *ISME J* 2011;**5**:1438–50.

Walsby AE. Mucilage secretion and the movements of blue-green algae. *Protoplasma* 1968;**65**:223–38.

Walter MR, Bauld J, Brock TD. Microbiology and morphogenesis of columnar stromatolites (*Conophyton, Vacerrilla*) from hot springs in Yellowstone National Park. *Developments in Sedimentology*. Vol 20. 1976, 273–310.

Wang Y, Qian PY. Conservative fragments in bacterial 16S rRNA genes and primer design for 16S ribosomal DNA amplicons in metagenomic studies. *PLoS One* 2009;**4**:e7401.

Widder S, Allen RJ, Pfeiffer T *et al.* Challenges in microbial ecology: building predictive understanding of community function and dynamics. *ISME J* 2016;**10**:2557–68.

Yang C, Zhang W, Liu R *et al.* Phylogenetic diversity and metabolic potential of activated sludge microbial communities in full-scale wastewater treatment plants. *Environ Sci Technol* 2011;**45**:7408–15.

Yu Y, Lee C, Kim J *et al.* Group-specific primer and probe sets to detect methanogenic communities using quantitative real-time polymerase chain reaction. *Biotechnol Bioeng* 2005;**89**:670–9.

Supplementary information

Initial type and abundance of cyanobacteria determine morphotype development of phototrophic ecosystems

Esmee Desirée Joosten, Jérôme Hamelin, Kim Milferstedt

INRAE, Univ Montpellier, LBE, 102 Avenue des Etangs, 11100, Narbonne, France

Progression of photogranulation

Closed microplates and vials with fresh activated sludge were hydrostatically incubated on the document table of a desktop scanner with the scanner lid removed. We followed the transformation of activated sludge into a morphotype using high-throughput time-lapse imaging and automated image analysis (Joosten, Hamelin and Milferstedt 2020). No significant differences were obtained for onset of contraction, contraction speed (slope) and final granule diameter compared to the control for additions up to $1.2 \cdot 10^4$ 16S rRNA gene copies·mL^{-1} of cyanobacteria (**Figure S 1**). For larger cyanobacterial doses, final granule diameters were significantly larger than the control (p-value 0, t-test). Bioaugmentation shifted morphotype development when a sufficient amount of biomass was added.

Description of biomass for augmentations

Photogranules for augmentations were produced in hydrostatic batch cultivation and bioreactors using published procedures (Milferstedt *et al.* 2017; Joosten, Hamelin and Milferstedt 2020).

Complex phototrophic communities

Phototrophic communities for augmentations originated from homogenization of the manually separated and pooled outer layers of hydrostatically produced photogranules (addition **i**), photogranules from a bioreactor (addition **ii**) and a hydrostatically produced photogranule after augmentation with the culture collection strain SAG 1459-3 (addition **ix**). Addition **iii** originated from direct homogenization of entire photogranules from a bioreactor.

The dominant cyanobacterium in the complex phototrophic communities was a *Tychonema* sequence type based on the 23S rRNA gene amplicon sequences (additions **i**, **ii**, **ix**; identical sequence type in all three additions). The dominant cyanobacterium in addition (**iii**) could not be classified based on its 23S rRNA gene amplicon sequence. Based on its 16S rRNA gene amplicon sequence, it is affiliated with *Pantanalinema*.

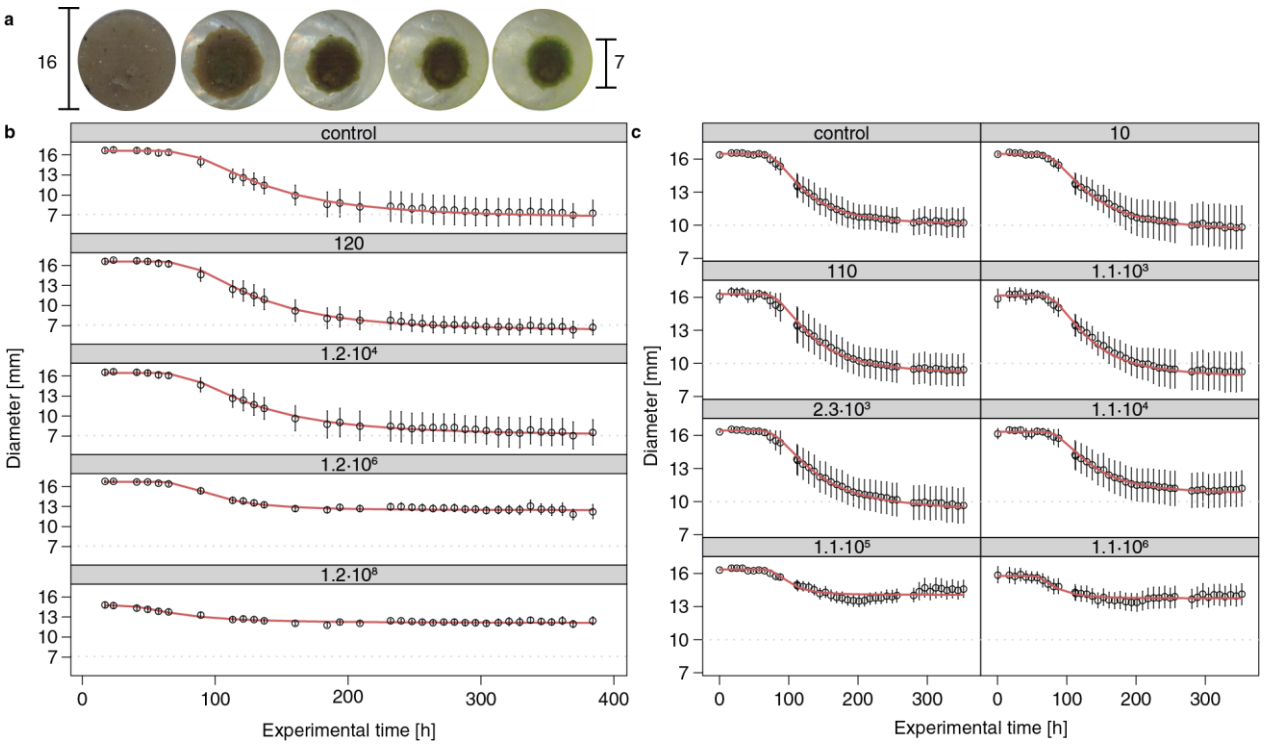

Figure S 1. Progression of photogranulation. (a) Photogranulation is quantified as biomass contraction, i.e. the decrease in diameter over time, measured through the bottom of microplate wells according to a published protocol (Joosten, Hamelin and Milferstedt 2020). (b) Photogranulation progression for activated sludge 1 augmented with addition i: homogenized outer layers of hydrostatically produced photogranules. Biomass contraction is displayed as a function of the concentration of the most dominant sequence type in the addition, Tychonema, expressed in 16S rRNA gene copies·mL-1 (values noted in the grey boxes at the top of each panel). Initially, the biomass covers the entire bottom, i.e. 16 mm. During successful photogranulation, the biomass contracts and forms an photogranule with a minimum diameter of approximately 7 mm. The biomass contracts minimally when a mat is formed (13 mm). Each graph panel represents the average of 17-20 replicates. Red lines represent Weibull distributions fitted to the data. Error bars represent standard deviations. (c) Photogranulation progression for activated sludge 2 augmented with addition ii: homogenized outer layers of photogranule from a bioreactor. During successful photogranulation, the biomass contracts and forms an photogranule with a minimum diameter of approximately 10 mm. The biomass contracts minimally when a mat is formed (14 mm). Each graph panel represents the average of 11-12 replicates.

Xenic cyanobacterial strains

Xenic cyanobacterial strains for augmentations were ordered from a culture collection, *i.e.* the strain *Oscillatoria lutea* SAG 1459-3 (addition **iv**), or isolated from different mature photogranules (additions **v-viii**). Single cyanobacterial filaments were isolated at the Muséum National d'Histoire Naturelle (MNHN), Paris, France, from (a) hydrostatically produced photogranules by direct selection from a piece of the biomass suspended in a water droplet (additions **v-vi**); (b) photogranules from a bioreactor by selection from a medium-solid agar plate after filaments had separated from the biomass by photomovement (additions **vii-viii**) (Rippka 1988). Hydrostatically produced photogranules resulted from the transformation of activated sludge in closed 24-well microplates or 10 ml vials that were hydrostatically incubated under constant warm white LED or incandescent light illumination (60 µmol·m^{-2}·s^{-1} PAR). Photogranules from a bioreactor were

produced in a sequencing batch photobioreactor (Ouazaite *et al.* 2021) or continuously stirred tank reactor (Safitri *et al.* 2021).

The cyanobacterial strain in addition **v** was an unclassified *Phormidiaceae* strain based on its 23S rRNA gene amplicon sequence, and as *Kamptonema* based on its 16S rRNA gene amplicon sequence. We call this strain the *Kamptonema*-like strain. The cyanobacterial strains in additions **vi** and **vii** were closely related to *Planktothrix agardhii* NIVA CYA 15 and *Nodosilinea nodulosa* PCC 7104 based on their respective 16S and 23S rRNA gene amplicon sequences. We therefore call them, respectively, *Planktothrix*- and *Nodosilinea*-like strain. The cyanobacterial strain in addition **viii** could not be classified based on its 23S rRNA gene amplicon sequence. It is affiliated with *Oscillatoria* SAG 1459-8 based on its 16S rRNA gene amplicon sequence.

It should be noted that the taxonomy of cyanobacteria is under constant revision as scientists are working towards a consensus approach (Palinska and Surosz 2014). True taxonomic classification should therefore not be based on names given to sequences alone, but on a combination of molecular and morphological studies (Komárek 2006).

We determined trichome cell width of the cyanobacterial strains in the additions to be consistent with the literature by ImageJ analysis of microscopic images, except for addition **viii** (**Table S1**). This cyanobacterial strain does not resemble an *Oscillatoria*-like organism based on its cell width. Its trichomes were too thin (1.3-1.4±0.2 µm) compared to typical *Oscillatoria* trichomes of ~3.5 µm (Kruschel and Castenholz 1998) (**Table S1**). We call the cyanobacterial strain in addition **viii** therefore the unclassified cyanobacterium strain. Performing a BLAST search on the NCBI nr/nt database, the 23S rRNA gene amplicon sequence was 99% similar to a sequence from an algal bloom (Sequence ID: GQ994598.1) and from a previous photogranule experiment in our laboratory (Milferstedt *et al.* 2017) (Sequence ID: KY920274.1). The 16S rRNA gene amplicon sequence was identical to sequences classified as *Tildeniella torsiva* (Sequence ID: KY498229.1) and *Jaaginema geminatum* (Sequence ID: KM019979.1), which both have filament widths comparable to our unclassified cyanobacterium strain (**Table S1**).

Table S1. Filament width of cyanobacterial strains in Z8 and BG-11 medium. Filament is determined from microscopic images by ImageJ analysis and results are compared to the literature. "n.a." means "not available".

Augmentation	Z8 medium		BG-11 medium		Literature
Oscillatoria lutea SAG 1459-3 (**iv**)	4.0±0.3 µm	n=27	3.5±0.5 µm	n=49	~3.5 µm (Kruschel and Castenholz 1998)
Kamptonema-like strain (**v**)	5.6±0.4 µm	n=31	5.2±0.6 µm	n=76	2.5-5.3 µm (Strunecky, Komárek and Šmarda 2014); 3.5–5 µm (*K. okenii*) (Shiels *et al.* 2019)
Planktothrix-like strain (**vi**)	5.6±0.4 µm	n=17	4.8±0.6 µm	n=21	2.3-9.8 µm (*P. agardhii*) (Komárek and Komárkova 2004)
Nodosilinea-like strain (**vii**)	1.6±0.3 µm	n=7	1.1±0.2 µm	n=91	1.2-2.4 µm (*N. nodulosa*) (Radzi *et al.* 2019); 1.1–1.5 µm (*N. nodulosa*) (Brito *et al.* 2017)
Unclassified cyanobacterium strain (**viii**)	1.4±0.2 µm	n=14	1.3±0.2 µm	n=40	1.4-1.9 µm *Tildeniella torsiva* (Mai *et al.* 2018); 2.3–3.3 µm *Jaaginema geminatum* (Gupta 2017)
Tychonema-like strain (**ix**)	n.a.	n.a.	5.2±0.6 µm	n=165	6.5-8 µm (*T. decoloratum*) (Shiels *et al.* 2019)

Filamentous cyanobacteria from photogranules from bioreactors were smaller in diameter than those from hydrostatic photogranules. In bioreactors, there are hydrodynamic forces that promote granulation, *e.g.* hydrodynamic shear force. In hydrostatic photogranulation, these external driving forces are absent and photogranulation results uniquely from the microbial activities.

Abundant bacteria in final morphotypes

Most abundant bacterial sequence types in the final morphotypes were affiliated with:

- Class Gammaproteobacteria, Genus Luteimonas detected in 49 of 68 samples at an average abundance of 5.2%±6.4%
- Class Betaproteobacteria, Genus Hydrogenophaga in 39 of 68 samples at 3.5%±3.1%
- Class Gemmatimonadetes, Family Gemmatimonadaceae in 36 of 68 samples at 2.4%±2.1%.

BLAST searches did not result in better taxonomic identifications.

Proportion of morphotype-forming strains in final communities

We investigated how mat-, hemispheroid-, and photogranule-forming cyanobacteria were represented in the final communities of the final morphotypes that resulted from the transformation of untreated sludge and sludge augmented with phototrophic communities or cyanobacterial strains (**Figure S 2**).

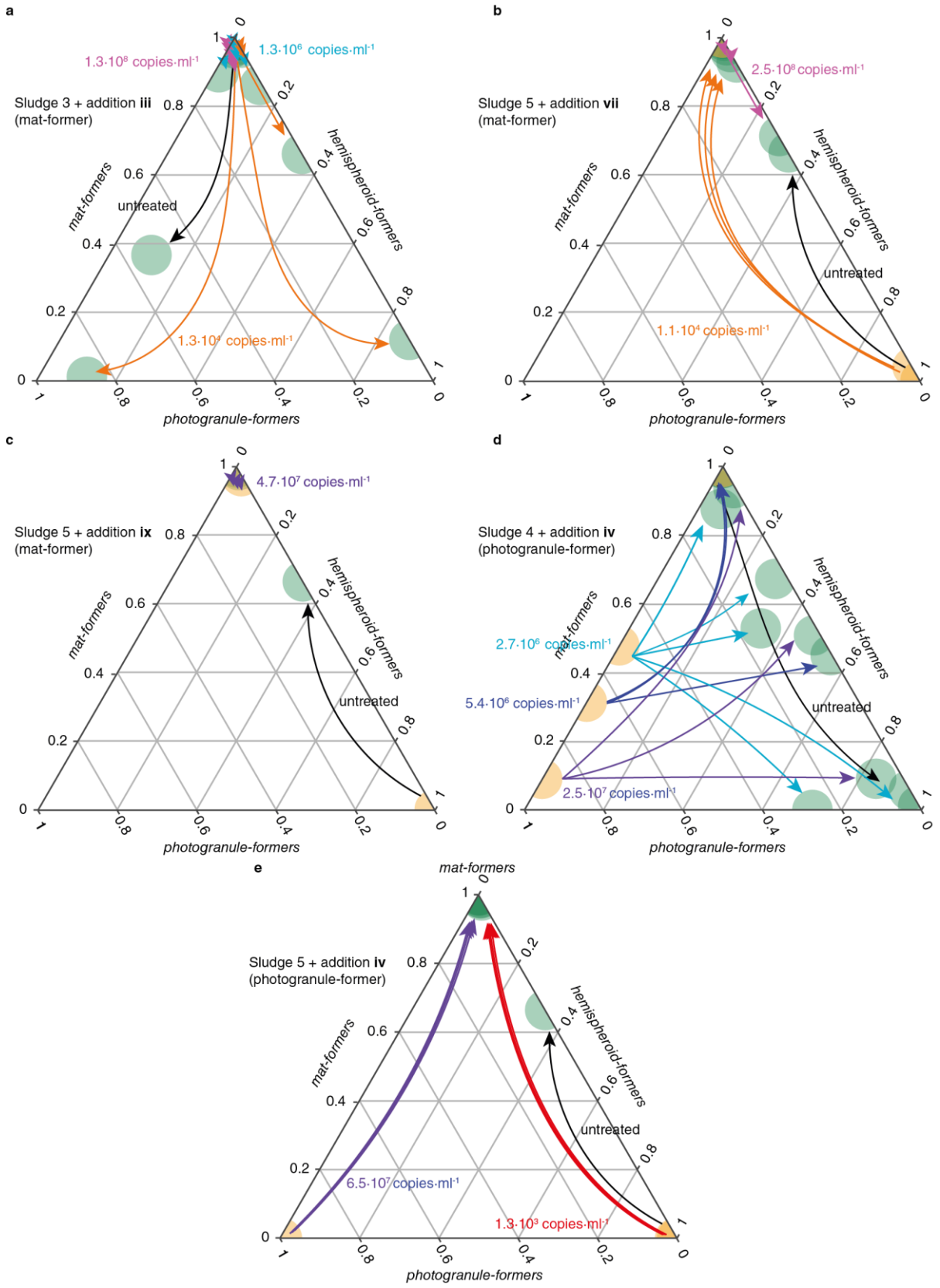
a
Sludge 3 + addition iii
(mat-former)
1.3·10⁸ copies·ml⁻¹
1.3·10⁶ copies·ml⁻¹
1.3·10³ copies·ml⁻¹
untreated
b
Sludge 5 + addition vii
(mat-former)
2.5·10⁸ copies·ml⁻¹
1.1·10⁴ copies·ml⁻¹
untreated
c
Sludge 5 + addition ix
(mat-former)
4.7·10⁷ copies·ml⁻¹
untreated
d
Sludge 4 + addition iv
(photogranule-former)
2.7·10⁶ copies·ml⁻¹
5.4·10⁶ copies·ml⁻¹
2.5·10⁷ copies·ml⁻¹
untreated
e
Sludge 5 + addition iv
(photogranule-former)
6.5·10⁷ copies·ml⁻¹
1.3·10³ copies·ml⁻¹
untreated
mat-formers
hemispheroid-formers
photogranule-formers

Figure S 2. Representative changes in proportion of mat-, hemispheroid- and photogranule-formers from the inoculum to the final morphotype communities. (a) Sludge 3 augmented with addition iii, (b) sludge 5 with addition vii, (c) sludge 5 with addition ix, (d) sludge 4 with addition iv and (e) sludge 5 augmented with addition iv. Results are based on 23S rRNA gene amplicon sequencing and cyanobacterial qPCR. Initial activated sludge is shown in orange and final morphotypes in green. Untreated control is represented by a black arrow. Increasing cyanobacterial additions are indicated by colored arrows. We used the same color for replicates on the same image (n=5 for sludge 3; n=3-5 for sludge 4; n=2-3 for sludge 5) and for additions with the same order of magnitude between images.

Growth of cyanobacterial strains in culture medium

We cultivated xenic cyanobacterial strains in 50 ml Z8 and BG-11 medium at 12/12-hour light/dark cycles at 11 $\mu mol \cdot m^{-2} \cdot s^{-1}$ PAR. We measured their dry weight after three months to assess how well they grow on the culture media (**Table S2**).

Table S2. Dry weight of cyanobacterial strains cultivated in Z8 and BG-11 media over 82 days.

	Dry weight (mg) in Z8	**Dry weight (mg) in BG-11**
Planktothrix-like strain	8±1	27±14
Kamptonema-like strain	12±1	6±6
Nodosilinea-like strain	36±4	33±6
Unclassified cyanobacterium strain	20±3	30±5
Oscillatoria lutea SAG 1459-3	46±6	54±8

References

Brito Â, Ramos V, Mota R *et al.* Description of new genera and species of marine cyanobacteria from the Portuguese Atlantic coast. *Mol Phylogenet Evol* 2017;**111**:18–34.

Gupta P. New record of Cyanoprokaryotes from West Bengal in Maldah district. *Trop Plant Res* 2017;**4**:421–32.

Joosten ED, Hamelin J, Milferstedt K. Simple time-lapse imaging for quantifying the hydrostatic production of oxygenic photogranules. *Bio-Protocol* 2020;**10**:e3784.

Komárek J. Cyanobacterial taxonomy: current problems and prospects for the integration of traditional and molecular approaches. *Algae* 2006;**21**:349–75.

Komárek J, Komárkova J. Taxonomic review of the cyanoprokaryotic genera *Planktothrix* and *Planktothricoides*. *Czech Phycol Olomouc* 2004:1–18.

Kruschel C, Castenholz RW. The effect of solar UV and visible irradiance on the vertical movements of cyanobacteria in microbial mats of hypersaline waters. *FEMS Microbiol Ecol* 1998;**27**:53–72.

Mai T, Johansen JR, Pietrasiak N *et al.* Revision of the *Synechococcales* (Cyanobacteria) through recognition of four families including Oculatellaceae *fam. nov.* and Trichocoleaceae *fam. nov.* and six new genera containing 14 species. *Phytotaxa* 2018;**365**:1–59.

Milferstedt K, Kuo-Dahab WC, Butler CS *et al.* The importance of filamentous cyanobacteria in the development of oxygenic photogranules. *Sci Rep* 2017;**7**:17944.

Ouazaite H, Milferstedt K, Hamelin J *et al.* Mapping the biological activities of filamentous oxygenic photogranules. *Biotechnol Bioeng* 2021;**118**:601–11.

Palinska KA, Surosz W. Taxonomy of cyanobacteria: a contribution to consensus approach. *Hydrobiologia* 2014;**740**:1–11.

Radzi R, Muangmai N, Broady P *et al. Nodosilinea signiensis* sp. nov. (Leptolyngbyaceae, Synechococcales), a new terrestrial cyanobacterium isolated from mats collected on Signy Island, South Orkney Islands, Antarctica. *PLoS One* 2019;**14**:e0224395.

Rippka R. Isolation and Purification of Cyanobacteria. *Methods Enzymol* 1988;**167**:3–27.

Safitri AS, Hamelin J, Kommedal R *et al.* Engineered methanotrophic syntrophy in photogranule communities removes dissolved methane. *Water Res X* 2021;**12**:100106.

Shiels K, Browne N, Donovan F *et al.* Molecular characterization of twenty-five marine cyanobacteria isolated from coastal regions of Ireland. *Biology (Basel)* 2019;**8**:59.

Strunecky O, Komárek J, Šmarda J. *Kamptonema* (*Microcoleaceae, Cyanobacteria*), a new genus derived from the polyphyletic *Phormidium* on the basis of combined molecular and cytomorphological markers. *Preslia* 2014:193–207.